Towards Understanding Hemispheric variations in Enceladus' Ice Shell: Variable Surface Temperatures, Convection, and Yielding. M. B. Weller, L. Fuchs, T. W. Becker, and K. M. Soderlund, Institute for Geophysics, Jackson School of Geosciences, The University of Texas at Austin, Austin, TX (mbweller@ig.utexas.edu, lfuchs@ig.utexas.edu, twb@ig.utexas.edu, krista@ig.utexas.edu)

Introduction: Despite Enceladus' small size, observations reveal it as one of the more geologically active bodies in the Solar System. Its surface is heavily deformed, including ridges, grooves, grabens, rifts, and folds that cover a significant fraction of the planet [1-3]. Notably at a hemispheric scale, there is evidence of a dichotomy between the south (the so-called South Polar Terrain – SPT), and the remainder of the icy satellite. While the origin of the SPT has spurred significant debate, ranging from internal convective processes [e.g., 4-9], oceans and tides to impacts [e.g., 10-11], its existence suggests some form of localization process(es). Here, we use the mantle convection code CitcomS to address the effects of latitudinally variable surface temperature (due to differences in solar heating) for a range of internal heating rates (as proxy for tidal heating), and yield strengths on the convective vigor and planform within Enceladus' ice shell.

Numerical Methods: The governing equations of mass, momentum, and energy conservation, assuming infinite Prandtl number and Boussinesq fluid approximation, are given in non-dimensional form by:

$$u_{i,i} = 0 \quad (1)$$

$$-P_{,i} + \left(\eta\left(u_{i,j} + u_{j,i}\right)\right)_{,j} + RaT\delta_{ir} = 0 \quad (2)$$

$$T_{,t} + u_i T_{,i} = T_{,ii} + Q \quad (3)$$

where u is the velocity, P dynamic pressure, η the viscosity, Ra the Rayleigh number, T the temperature, δ_{ij} the Kronecker delta, Q the heat production rate, i and j represent spatial indices, r is a unit vector in the radial direction, t is time, and the form $X_{,y}$ represents the derivative of X with respect to y. Repeated indices imply summation. Eqs. (1-3) are solved using the well benchmarked finite element code CitcomS [e.g., 12 – 14].

Subsets of our models include temperature-dependent viscosity, which follows as:

$$\eta(T) = \eta_0 \exp\left(A\left[\frac{1}{T+1} - \frac{1}{2}\right]\right) \quad (4)$$

Here, η_0 is the pre-exponential factor and is set to unity. The dimensional reference viscosity at the base of ice shell is estimated to be ~10^{13} to ~10^{15} Pa s [e.g., 3, 14]. The rheological parameter, A, is chosen to give a variation in viscosity, from the base of the domain to the surface, of 10^4 – 10^5, which are reasonable approximations based on estimates of SPT surface viscosities of O($10^{17–19}$ Pa s) [3]. The Rayleigh number at the base of the ice shell is taken as $3\cdot10^5$ or $3\cdot10^6$ for η_0 =10^{15} and 10^{14} Pa·s, respectively. Internal heating rates are varied from ~49 to ~0 (corresponding to heating rates between $2.3\cdot10^{-10}$ W kg^{-1} and ~10^{-11} [6] (Q = 49 – 2), as well as additional pure basal heating conditions). Internal heating rates are currently uniform in the model domain. Total ice shell thickness is taken as 60 km as an upper bound (giving a core fraction of ~0.762 for these models). Some models allow for plastic yielding of the surface, with non-dimensional yielding values set from $1\cdot10^5$ – $1\cdot10^7$ (corresponding to yield strength values of ~3 kPa – 3 MPa, in agreement with estimates of ice strengths of ~1 MPa [15]). The modeling domain consists of 65×65×33 nodes for each of the 12 spherical caps.

The surface temperature (T_s) of Enceladus varies due to solar insolation from equator to poles. The base of the ice shell may reach temperatures of ~273 K (assuming a pure water ocean [16]). We have modified CitcomS to allow for continuous variation in the surface temperature boundary conditions from pole to equator (a basal non-dimensional temperature of unity, equatorial temperature of 0.165, and a polar temperature of zero).

Results: To isolate the effects of a pole to equator variation in T_s, we first consider models that start isoviscous for variable Q and subsequently add temperature dependent viscosity variation of up to 10^4 for both cases of constant and variable T_s (Q = 0 cases shown in Figure 1A: isoviscous, 1B: temperature-dependent viscosity). Both cases are designed to operate at the same effective Ra (average T_s is identical for each case).

With regard to the isoviscous cases (Figure 1A), for all Q ranges, the application of variable T_s tends to disrupt the planform of convection compared to constant T_s cases. The equatorial region favors warm upwellings, while polar regions favor cold downwellings, leading to a thinning equatorial and thickening polar boundary layer, respectively.

Additionally, polar (z-axis) oriented downwelling zones may develop (downwelling velocity low along +y-axis limb, Figure 1A). Bulk system velocities are effectively identical between both systems (< 0.5% misfit), indicating the effective Ra is nearly identical, and that applying variable T_s results in the reorientation of convective cells to reflect the changing driving forces of the boundary conditions (from variable T_s).

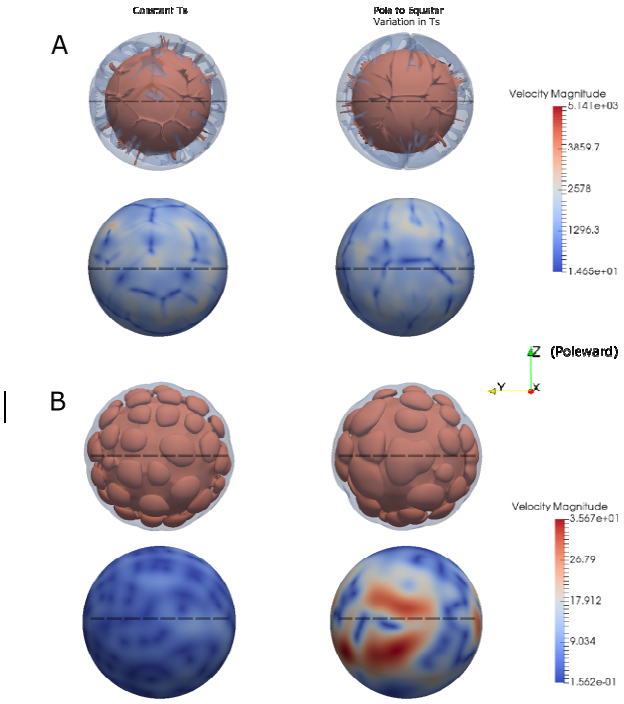

Figure 1: Results showing iso-temperature surfaces (top rows; red: 0.8; transparent blue: 0.3), and surface velocity magnitude for basally heated systems (Q = 0) and Ra = $3{\cdot}10^5$, for A) isoviscous, and B) a temperature dependent viscosity variation of 10^4. The left-hand side of both figures indicates constant T_s while the right is a pole to equator variation in T_s of 0.165. Constant T_s cases are modified to the same effective Ra as variable T_s cases (e.g., bulk system velocities are within ~0.5% of each other). Poles are oriented along the z-axis (top to bottom of plots), dashed line is equatorial plane.

Next, we consider the application of temperature dependence to the isoviscous systems (Figure 1B). The equatorial region slightly favors larger convective cells, whereas the polar regions tend to favor smaller cells. In general, a "patchwork" network of horizontal surface velocities tend to be maximal near the equatorial regions. Maximum surface velocities may reach as high as 20% of the bulk model velocity, ~4x larger than the fixed case, indicating regions of a "local" sluggish lid, leading to a greater deviation (< 5% misfit) in bulk system velocities between cases. Boundary layers are highly variable, with maxima occurring in the poles and the mid-latitudes along the +y-axis (region of depressed temperatures and of higher surface velocities).

Strain rates in the higher surface velocity regions (~20% of the surface area) are inferred to be ~10^{-14} s^{-1}, with the slower regions approaching the constant T_s case of O(10^{-17}) s^{-1}, in reasonable agreement with estimated strain rates for Enceladus [17, 18]. These results indicate that variable T_s results in a significant alteration of surface and internal dynamics within high viscosity contrast regimes (e.g., in what would nominally be a classified as a stagnant-lid).

We lastly consider the effects of plastic yielding (Figure 2). A non-dimensional yield strength of 10^7 (3 MPa) was chosen to allow for stagnant-lid behavior for the constant T_s case. The same yield strength in the variable T_s system results in continuous hemispheric scale downwelling, encircling ~ 30–40% of the surface, with a linear upwelling zone, comprising ~ 8–12% of the surface area and oriented near but offset from, the +z-axis. The downwelling zone roughly correlates to, and is suggestive of, the along polar (z-axis) oriented downwelling zones in the isoviscous case in Figure 1A, suggesting that orientations of convective cells can become oriented pole-ward, and facilitate failure near polar zones (through going failure zone through polar region, Figure 2). The size and general orientation of this hemispheric scale feature is evocative for the formation mechanism of the SPT. Future work will explore additional yielding at variable Q as well as strain tracking, which will allow for a strain accumulation, or "memory", within the ice shell.

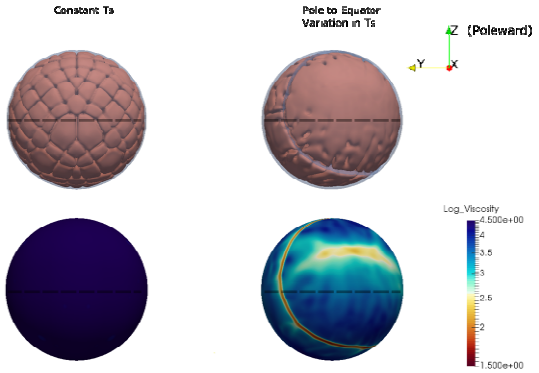

Figure 3: Results showing iso-temperature surfaces (top row; red: 0.8; transparent blue: 0.3), and surface viscosity plots for mixed heated systems (Q = 49) with a Ra = $3{\cdot}10^6$, and a yield strength of 10^7 (~3 MPa). Poles are oriented along the z-axis (top to bottom of plots), dashed line is equatorial plane.

References: [1]. Kargel, J.S., & S. Pozio (1996) Icarus 119, 385-404. [2]. Porco, C.C., et al. (2006) Science 311, 1393-1401. [3] Barr, A.C. & L.J. Preuss (2010) Icarus 208, 499–503. [4] Barr, A.C. (2008) JGR 113, doi:10.1029/2008JE003114. [5] Roberts, J.H., & F.. Nimmo (2008) GRL 35. [6] O'Neill, C., & F. Nimmo (2010) Nature Geoscience. [7] Han, L., et al., (2012) Icarus 218, 320-330. [8] Showman, A.P. et al., (2013) Geophys. Res. Lett. 40. [9] Rozel, A. et al., (2014) JGR 19, 416–439. [10] Collins, G.C., & J.C. Goodman (2007) Icarus 189, 72-82. [11] Tobie, G., et al. (2008) Icarus doi:10.1016/ j.icarus.2008.03.008. [12] L.N. Moresi & V.S. Solomatov (1995), Phys. Fluids,7 (9), 2154-2162. [13] Zhong, S., et al. (2000), JGR, 105, 11063–11082. [14] Tan, E., et al. (2006), G3, 7, Q06001. [15] Beeman, M. et al. 1988, JGR, 93, 10.1029/JB093iB07p07625. [16] Glein, C. et al., GCA, 2016. [17] Durham, W.B. & L.A. Stern (2001) Annu. Rev. Earth Planet. Sci. 29, 295–330. [18] Barr, A.C., & W.B. McKinnon (2007) GRL 34.